Baryon resonance analysis from MAID*

L. Tiator[1;1)] D. Drechsel[1] S.S. Kamalov[2] M. Vanderhaeghen[1]

1 (Institut für Kernphysik, Universität Mainz, D-55099 Mainz, Germany)
2 (Bogoliubov Laboratory for Theoretical Physics, JINR, Dubna, 141980 Moscow Region, Russia)

Abstract The unitary isobar model MAID2007 has been used to analyze the recent data of pion electroproduction. The model contains all four-star resonances in the region below $W = 2$ GeV and both single-Q^2 and Q^2 dependent transition form factors could be obtained for the Delta, Roper, $D_{13}(1520)$, $S_{11}(1535)$, $S_{31}(1620)$, $S_{11}(1650)$, $D_{15}(1675)$, $F_{15}(1680)$ and $P_{13}(1720)$. From the complete world data base, including also π^- data on the neutron, also Q^2 dependent neutron form factors are obtained. For all transition form factors we also give convenient numerical parameterizations that can be used in other reactions. Furthermore, we show how the transition form factors can be used to obtain empirical transverse charge densities and our first results are given for the Roper, the S_{11} and D_{13} resonances.

Key words pion photo- and electroproduction, non-strange baryons, transition form factors

PACS 14.20.Gk, 13.30.Eg, 13.75.Gx

1 Introduction

Our knowledge about the excitation spectrum of the nucleon was originally provided by elastic pion-nucleon scattering. All the resonances listed in the Particle Data Tables[1] have been identified by partial-wave analyses of this process with both Breit-Wigner and pole extraction techniques. From such analyses we know the resonance masses, widths, and branching ratios into the πN and $\pi\pi$N channels. These are reliable parameters for the four-star resonances, with only few exceptions. In particular, there remains some doubt about the structure of two prominent resonances, the Roper $P_{11}(1440)$, which appears unusually broad, and the $S_{11}(1535)$, where the pole can not be uniquely determined, because it lies close to the ηN threshold.

On the basis of these relatively firm grounds, additional information can be obtained for the electromagnetic (e.m.) γNN* couplings through pion photo- and electroproduction. These couplings are described by electric, magnetic, and charge transition form factors (FFs), $G^*_E(Q^2)$, $G^*_M(Q^2)$, and $G^*_C(Q^2)$, or by linear combinations thereof as helicity amplitudes $A_{1/2}(Q^2)$, $A_{3/2}(Q^2)$, and $S_{1/2}(Q^2)$. So far we have some reasonable knowledge of the transverse amplitudes $A_{1/2}$ and $A_{3/2}$ at the real photon point, which are tabulated in the Particle Data Tables. For finite Q^2 the information found in the literature is scarce and until recently practically nonexistent for the longitudinal amplitudes $S_{1/2}$.

A big step forward was done during the last decade by the experiments at JLab, where electroproduction of π^0 and π^+ have been measured on the proton. Most of these experiments did not use polarization degrees of freedom, but the virtual photon in electroproduction always carries longitudinal and transverse polarizations which are accessible in experiments with large azimuthal angle coverage. In addition, also some experiments, especially in the $\Delta(1232)$ region were performed with polarized electrons, polarized target and even an almost complete experiment was done in Hall A with 16 unpolarized and recoil polarization observables at $Q^2 = 1.0$ GeV^2.

With our unitary isobar model MAID we have analyzed the electroproduction data and have obtained transition form factors for all 13 four-star resonances below $W = 2$ GeV. For the proton target in most cases we could obtain both single-Q^2 and Q^2-dependent transition form factors, for the neutron target we parameterized the Q^2 dependence in a simpler form as far as the existing data from the world data base

Received 7 August 2009

* Supported by Deutsche Forschungsgemeinschaft through SFB 443 and joint Russian-German Heisenberg-Landau program

1) E-mail: tiator@kph.uni-mainz.de

allows.

Furthermore, the precise e.m. FF data, extracted from experiment, allow us to map out the quark charge densities in a baryon. It was shown possible to define a proper density interpretation of the form factor data by viewing the baryon in a light-front frame. This yields information on the spatial distribution of the quark charge in the plane transverse to the line-of-sight. In this way, the quark transverse charge densities were mapped out in the nucleon[2, 3], and in the deuteron[4] based on empirical FF data. To understand the e.m. structure of a nucleon resonance, it is of interest to use the precise transition FF data to reveal the spatial distribution of the quark charges that induce such a transition. In this way, using the empirical information on the $\mathrm{N}\to\mathrm{N}^*$ transition form factors from the MAID analysis[5], the $\mathrm{N}\to\Delta(1232)$ transition charge densities have been mapped out in Ref. [3] and the $\mathrm{N}\to\mathrm{N}^*(1440)$ in Ref. [6]. In this work, we will extend this method to map out the quark transition charge densities inducing the $\mathrm{N}\to S_{11}(1535)$ and $\mathrm{N}\to D_{13}(1520)$ e.m. excitations.

2 The MAID ansatz

In the spirit of a dynamical approach to pion photo- and electroproduction, the T-matrix of the unitary isobar model is set up with the following ansatz

$$t_{\gamma\pi}(W)=t^{\mathrm{B}}_{\gamma\pi}(W)+t^{\mathrm{R}}_{\gamma\pi}(W) \tag{1}$$

of a background and a resonance T-matrix, where each of them is individually unitary. This is a very important starting point that will allow us later to clearly separate resonance and background amplitudes within a Breit-Wigner concept.

For a specific partial wave the background T-matrix is set-up by a potential multiplied by pion nucleon scattering amplitudes in accordance with the K-matrix approximation,

$$t^{\mathrm{B},\alpha}_{\gamma\pi}(W,Q^2)=v^{\mathrm{B},\alpha}_{\gamma\pi}(W,Q^2)\,[1+\mathrm{i}t^{\alpha}_{\pi\mathrm{N}}(W)]\,, \tag{2}$$

where only the on-shell part of the pion nucleon rescattering is maintained and the off-shell part from pion loop contributions is neglected. At threshold it is well known that this is a bad approximation for γ,π^0 production, however in the resonance region it is well justified as the main contribution from pion loop effects is absorbed by the nucleon resonance dressing.

The background potential $v^{\mathrm{B},\alpha}_{\gamma\pi}(W,Q^2)$ is described by Born terms obtained with an energy dependent mixing of pseudovector-pseudoscalar πNN coupling and t-channel vector meson exchanges. The mixing parameters and coupling constants were determined from an analysis of nonresonant multipoles in the appropriate energy regions. In the latest version, MAID2007, the S, P, D and F waves of the background contributions are unitarized as explained above, where the pion-nucleon elastic scattering amplitudes, $t^{\alpha}_{\pi\mathrm{N}}=[\eta_\alpha\exp(2\mathrm{i}\delta_\alpha)-1]/2\mathrm{i}$, are described by the phase shifts δ_α and the inelasticity parameters η_α taken from the GWU/SAID analysis[7].

For the resonance contributions we follow Ref. [8] and assume Breit-Wigner forms for the resonance shape,

$$t^{\mathrm{R},\alpha}_{\gamma\pi}(W,Q^2)= \bar{\mathcal{A}}^{\mathrm{R}}_{\alpha}(W,Q^2)\,\frac{f_{\gamma\mathrm{N}}(W)\Gamma_{\mathrm{tot}}\,M_{\mathrm{R}}\,f_{\pi\mathrm{N}}(W)}{M^2_{\mathrm{R}}-W^2-\mathrm{i}M_{\mathrm{R}}\,\Gamma_{\mathrm{tot}}}\,\mathrm{e}^{\mathrm{i}\phi_{\mathrm{R}}}\,, \tag{3}$$

where $f_{\pi\mathrm{N}}$ is the usual Breit-Wigner factor describing the decay of a resonance R with total width $\Gamma_{\mathrm{tot}}(W)$ and physical mass M_{R}. The expressions for $f_{\gamma\mathrm{N}}$, $f_{\pi\mathrm{N}}$ and Γ_{tot} are given in Ref. [8]. The phase $\phi_{\mathrm{R}}(W)$ in Eq. (3) is introduced to adjust the total phase such that the Fermi-Watson theorem is fulfilled below two-pion threshold. For the S- and P-wave multipoles we extend this unitarization procedure up to $W=1400$ MeV. Because of a lack of further information, we assume that the phases ϕ_{R} are constant at the higher energies. In particular we note that the phase ϕ_{R} for the $P_{33}(1232)$ excitation vanishes at $W=M_{\mathrm{R}}=1232$ MeV for all values of Q^2. For this multipole we may even apply the Fermi-Watson theorem up to $W\approx 1600$ MeV because the inelasticity parameter η_α remains close to 1. For the D- and F-wave resonances, the phases ϕ_{R} are assumed to be constant and determined from the best fit.

While in the original version of MAID only the 7 most important nucleon resonances were included with mostly only transverse e.m. couplings, in our new version all 13 four-star resonances below $W=2$ GeV are included. These are $P_{33}(1232)$, $P_{11}(1440)$, $D_{13}(1520)$, $S_{11}(1535)$, $S_{31}(1620)$, $S_{11}(1650)$, $D_{15}(1675)$, $F_{15}(1680)$, $D_{33}(1700)$, $P_{13}(1720)$, $F_{35}(1905)$, $P_{31}(1910)$ and $F_{37}(1950)$.

3 Transition form factors

The resonance couplings $\bar{\mathcal{A}}^{R}_{\alpha}(W,Q^2)$ in most cases are independent of the total energy and depend only on Q^2. A typical energy dependence occurs in MAID2007 e.g. for the $\Delta(1232)$ resonance in terms of the virtual photon three-momentum $k(W,Q^2)$. For all other resonances which are discussed here, how-

ever, we can assume a simple Q^2 dependence, $\bar{\mathcal{A}}_\alpha(Q^2)$. They can be taken as constants in a single-Q^2 analysis, e.g. in photoproduction, where $Q^2=0$ but also at any fixed Q^2, where enough data with W and θ variation is available, see Table 1. Alternatively they can also be parameterized as functions of Q^2 in an ansatz like

$$\bar{\mathcal{A}}_\alpha(Q^2)=\bar{\mathcal{A}}_\alpha(0)(1+a_1Q^2+a_2Q^4+a_3Q^8)\,\mathrm{e}^{-b_1Q^2}\,. \quad (4)$$

With such an ansatz it is possible to determine the parameters $\bar{\mathcal{A}}_\alpha(0)$ from a fit to the world database of photoproduction, while the parameters a_i and b_1 can be obtained from a combined fitting of all electroproduction data at different Q^2. The latter procedure we call the "superglobal fit". In MAID the photon couplings $\bar{\mathcal{A}}_\alpha$ are direct input parameters. They are directly related to the helicity couplings $A_{1/2}, A_{3/2}$ and $S_{1/2}$ of nucleon resonance excitation. For further details see Ref.[5].

In Tables 2, 3 and 4 we give the numerical values of the parameters for our Q^2 dependent, "superglobal fits". Our parametrization of the $\Delta(1232)$ form factors are more complicated, in particular due to build-in requirements from low energy theorems in the long wavelength limit, details are discussed in Ref. [5].

Table 1. Database of pion electroproduction for energies above the Δ resonance up to $W=1.7$ GeV, used in our single-Q^2 transition form factor analysis.

reference	year	reaction	Q^2/GeV^2
Joo et al.[9]	2002	$p\pi^0$	0.4 – 1.8
Joo et al.[10]	2004	$n\pi^+$	0.4 – 0.65
Laveissiere et al.[11]	2004	$p\pi^0$	1.0
Egiyan et al.[12]	2006	$n\pi^+$	0.3 – 0.6
Ungaro et al.[13]	2006	$p\pi^0$	3.0 – 6.0
Park et al.[14]	2008	$n\pi^+$	1.7 – 4.5

Table 2. New parameterizations of our transition form factors, Eq. (4), for proton targets.

N*, Δ*		$\bar{\mathcal{A}}_\alpha(0)$ (10^{-3}GeV$^{-1/2}$)	a_1/GeV^{-2}	a_2/GeV^{-4}	a_3/GeV^{-8}	b_1/GeV^{-2}
$P_{11}(1440)$p	$A_{1/2}$	−61.4	0.871	−3.516	−0.158	1.36
	$S_{1/2}$	4.2	40.	0	1.50	1.75
$D_{13}(1520)$p	$A_{1/2}$	−27.4	8.580	−0.252	0.357	1.20
	$A_{3/2}$	160.6	−0.820	0.541	−0.016	1.06
	$S_{1/2}$	−63.5	4.19	0	0	3.40
$D_{15}(1675)$p	$A_{1/2}$	15.3	0.10	0	0	2.00
	$A_{3/2}$	21.6	1.91	0.18	0	0.69
	$S_{1/2}$	1.1	0	0	0	2.00
$F_{15}(1680)$p	$A_{1/2}$	−25.1	3.780	−0.292	0.080	1.25
	$A_{3/2}$	134.3	1.016	0.222	0.237	2.41
	$S_{1/2}$	−44.0	3.783	0	0	1.85
$D_{33}(1700)$	$A_{1/2}$	226.	1.91	0	0	1.77
	$A_{3/2}$	210.	0.88	1.71	0	2.02
	$S_{1/2}$	2.1	0	0	0	2.00
$P_{13}(1720)$p	$A_{1/2}$	73.0	1.89	0	0	1.55
	$A_{3/2}$	−11.5	10.83	−0.66	0	0.43
	$S_{1/2}$	−53.0	2.46	0	0	1.55

Table 3. Maid2007 parameterizations, Eq. (4), for proton targets ($a_2=a_3=0$).

N*, Δ*		$\bar{\mathcal{A}}_\alpha(0)$	a_1	b_1
$S_{11}(1535)$p	$A_{1/2}$	66.4	1.608	0.70
	$S_{1/2}$	−2.0	23.9	0.81
$S_{31}(1620)$	$A_{1/2}$	65.6	1.86	2.50
	$S_{1/2}$	16.2	2.83	2.00
$S_{11}(1650)$p	$A_{1/2}$	33.3	1.45	0.62
	$S_{1/2}$	−3.5	2.88	0.76

For all other resonances the parameters are listed in the three tables. Due to the 2008 π^+ data that have been recently included in our database, we find differences compared to our MAID2007 parametrization for the following 6 proton transition form factors to $P_{11}(1440)$, $D_{13}(1520)$, $D_{33}(1440)$, $D_{15}(1675)$, $F_{15}(1680)$ and $P_{13}(1720)$.

Above the third resonance region there is an energy gap between 1800—1900 MeV, where no four-star resonance can be found. Beyond this gap and up to 2 GeV three more four-star resonances, $F_{35}(1905)$, $P_{31}(1910)$ and $F_{37}(1950)$ are reported by the PDG, which are also included in MAID. In electroproduction nothing is practically known about these states

and we have just introduced their reported photon couplings, multiplied with a simple gaussian form factor, $\exp(-2.0\,Q^2/\mathrm{GeV}^2)$. In MAID their main role is to define a global high-energy behavior that is needed for applications with dispersion relations and sum rules. Future experiments in this region will give us the necessary information to map out these form factors in more details.

Table 4. Same as Table 3 for neutron targets.

N*		$\bar{\mathcal{A}}_\alpha(0)$	a_1	b_1
$P_{11}(1440)$n	$A_{1/2}$	54.1	0.95	1.77
	$S_{1/2}$	−41.5	2.98	1.55
$D_{13}(1520)$n	$A_{1/2}$	−76.5	−0.53	1.55
	$A_{3/2}$	−154.	0.58	1.75
	$S_{1/2}$	13.6	15.7	1.57
$S_{11}(1535)$n	$A_{1/2}$	−50.7	4.75	1.69
	$S_{1/2}$	28.5	0.36	1.55
$S_{11}(1650)$n	$A_{1/2}$	9.3	0.13	1.55
	$S_{1/2}$	10.	−0.50	1.55
$D_{15}(1675)$n	$A_{1/2}$	−61.7	0.01	2.00
	$A_{3/2}$	−83.7	0.01	2.00
	$S_{1/2}$	0	0	0
$F_{15}(1680)$n	$A_{1/2}$	27.9	0	1.20
	$A_{3/2}$	−38.4	4.09	1.75
	$S_{1/2}$	0	0	0
$P_{13}(1720)$n	$A_{1/2}$	−2.9	12.70	1.55
	$A_{3/2}$	−31.0	5.00	1.55
	$S_{1/2}$	0	0	0

3.1 First resonance region

The $\Delta(1232)P_{33}$ is the only nucleon resonance with a well-defined Breit-Wigner resonance position, $M_\mathrm{R} = 1232$ MeV, because it is an ideal single-channel resonance, where the Breit-Wigner position is identical to the K-matrix pole position. Therefore, and due to the Watson theorem, the Nucleon to $\Delta(1232)$ transition is the only case, where we can obtain the form factors in a practically model independent way.

Results for the $\Delta(1232)$ transitions have been discussed very often in recent years. The magnetic form factor is very well known up to high momentum transfer of $Q^2 = 10$ GeV^2 and can be parameterized in a surprisingly simple form

$$G_\mathrm{M}^*(Q^2) = 3\,G_\mathrm{D}(Q^2)\mathrm{e}^{-0.21Q^2/\mathrm{GeV}^2} \tag{5}$$

with the standard dipole form factor G_D. The electric and Coulomb form factors are much smaller and are usually given as ratios to the magnetic form factor. While there is agreement between different analyses on the E/M ratio, which is practically constant at a few percent with a negative sign the S/M ratio is also negative, but reaches large magnitudes of around 25% at the $Q^2 \approx 6$ GeV^2 in the JLab analysis, whereas in the MAID analysis the magnitude is only around 10% with an asymptotically almost zero slope as predicted in calculations by Buchmann[15] and Ji et al.[16].

3.2 Second resonance region

Above the two-pion threshold, we can no longer apply the two-channel unitarity and consequently the Watson theorem does not hold anymore. Therefore, the background amplitude of the partial waves does not vanish at resonance as this was the case for the $\Delta(1232)$ resonance. As an immediate consequence the resonance-background separation becomes model-dependent. In MAID2007 we choose to separate the background and resonance contributions according to the K-matrix approximation, Eqs. (2), (3). Furthermore, we recall that the absolute values of the helicity amplitudes are correlated with the values used for the total resonance width Γ_R and the single-pion branching ratio β_π, giving rise to additional uncertainties from these hadronic resonance parameters. On the experimental side, the data at the higher energies are no longer as abundant as in the Δ region. However, the large data set recently obtained mainly by the CLAS collaboration (see Table 1) enabled us to determine the transverse and longitudinal helicity couplings as functions of Q^2 for all the four-star resonances below 1800 MeV. These data are available in the kinematical region of 1100 MeV $< W <$ 1680 MeV and 0.4 GeV$^2 < Q^2 <$ 1.8 GeV^2.

The helicity amplitudes for the Roper resonance $P_{11}(1440)$ are shown in Fig. 1. Our latest super-global solution (solid lines) is in reasonable agreement with the single-Q^2 analysis. The figure shows a zero crossing of the transverse helicity amplitude at $Q^2 \approx 0.7$ GeV^2 and a maximum at the relatively large momentum transfer $Q^2 \approx 2.0$ GeV^2. The longitudinal Roper excitation rises to large values around $Q^2 \approx 0.5$ GeV^2 and in fact produces one of the strongest longitudinal amplitude we can find in our analysis. This answers the question raised by Li and Burkert[17] whether the Roper resonance is a radially excited 3-quark state or a quark-gluon hybrid, because in the latter case the longitudinal coupling should vanish completely.

Figure 2 shows our results for the $S_{11}(1535)$ resonance. The red single-Q^2 data points show our 2007 analysis, while the black triangles are the 2008 analysis of Ref. [18]. Our Q^2 dependent analysis describes all data points quite well, except for the longitudinal form factor in the region around $Q^2 = 2$ GeV^2.

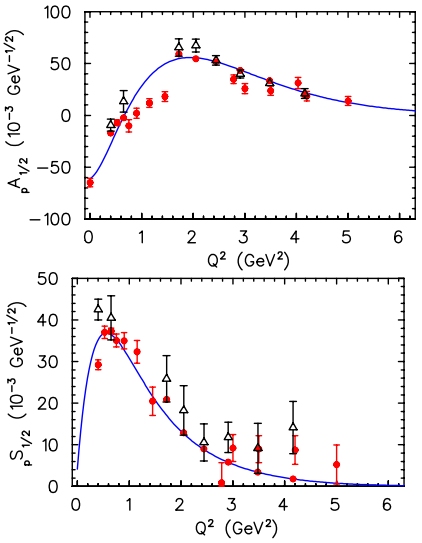

Fig. 1. Transverse and longitudinal form factors of the $P_{11}(1440)$ Roper resonance. The red circles are the MAID analysis of 2007[5] and 2008, and the black triangles are the 2008 JLab analysis[18]. The data point of the transverse form factor at $Q^2 = 0$ is the PDG value[1].

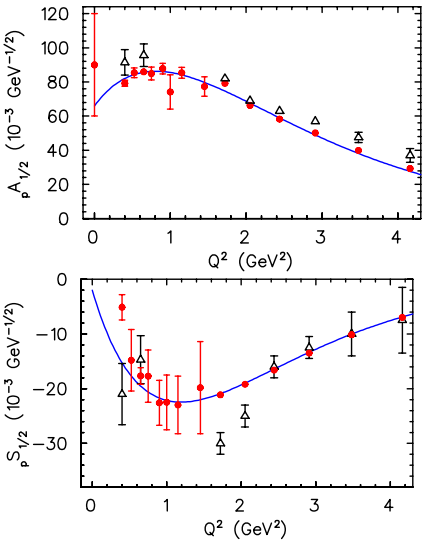

Fig. 2. Transverse and longitudinal form factors of the $S_{11}(1535)$ resonance. Notation as in Fig. 1.

While the inclusion of the 2008 Park π^+ data[14] did not modify our 2007 solution for the S_{11} resonance, we find some significant deviations for the $D_{13}(1520)$ resonance, see Fig. 3. Also for this resonance the JLab partial wave analysis of 2008 agrees well with the MAID analysis for most cases, however a significant deviation remains for $A_{1/2}$ in the region of $Q^2 = 2$ GeV^2.

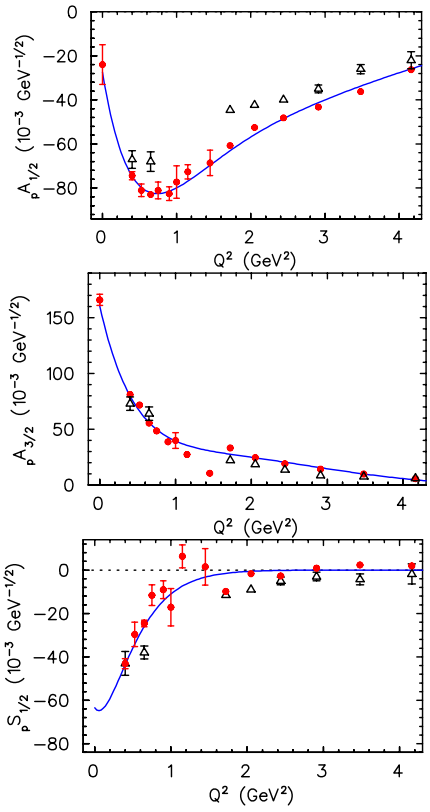

Fig. 3. Transverse and longitudinal form factors of the $D_{13}(1520)$ resonance. Notation as in Fig. 1.

3.3 Third resonance region

The $S_{31}(1620)$ is rather weakly excited by the electromagnetic probe. The PDG $A_{1/2}$ value at the photon point is only $(27 \pm 11) \cdot 10^{-3}$ GeV$^{-1/2}$ and below $Q^2 = 2$ GeV^2 we obtain similar values, at higher Q^2 it is consistent with zero, same as for the longitudinal form factor $S_{1/2}$.

Also for the second S_{11} resonance the longitudinal coupling is practically zero, but for the transverse form factor we find a solution shown in Fig. 4, which has the same shape as the first S_{11} resonance.

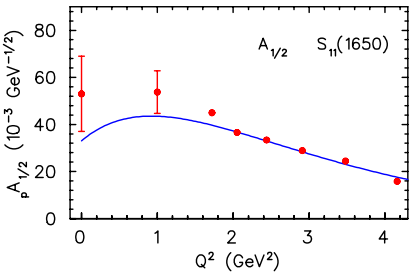

Fig. 4. Transverse form factors of the $S_{11}(1650)$ resonance. Notation as in Fig. 1.

A similar situation as for the D_{13} resonance we obtain for the $F_{15}(1680)$, shown in Fig. 5.

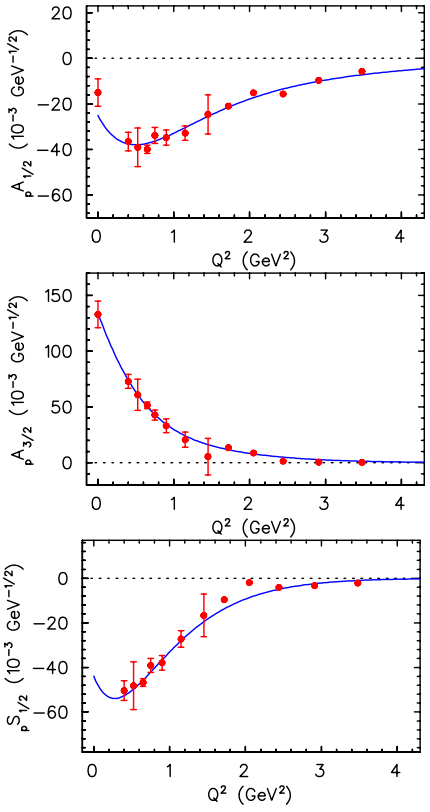

Fig. 5. Transverse and longitudinal form factors of the $F_{15}(1680)$ resonance. Notation as in Fig. 1.

For both resonances the helicity non-conserving amplitude $A_{3/2}$ dominates for real photons and with increasing values of Q^2, $A_{3/2}$ drops faster than the helicity conserving amplitude $A_{1/2}$. As a consequence the asymmetry

$$\mathcal{A}(Q^2) = \frac{|A_{1/2}|^2 - |A_{3/2}|^2}{|A_{1/2}|^2 + |A_{3/2}|^2} \tag{6}$$

changes rapidly from values close to -1 to values near $+1$ over a small Q^2 range. As a comparison, the asymmetry $\mathcal{A}$ for the $\Delta(1232)$ resonance is practically constant over this Q^2 range with a value ≈ -0.5. This again shows the special role of the Δ resonance, where the helicity conservation is not observed.

Finally, in Figs. 6 and 7 we show the situation for the $D_{15}(1675)$ and $P_{13}(1720)$ resonances, both without a significant longitudinal coupling. Unlike the situation discussed before, these two resonances have dominantly helicity 3/2 transitions, whereas the $A_{1/2}$ transition is consistent with zero. As for the $\Delta(1232)$ these are further examples for which the pQCD prediction for helicity conservation does not hold in the Q^2 region below 5 GeV^2.

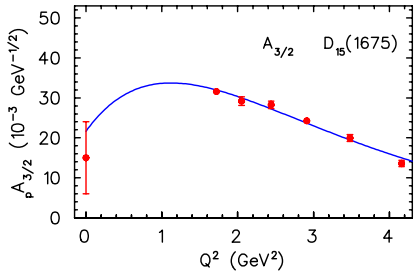

Fig. 6. Transverse form factor of the $D_{15}(1675)$ resonance. Notation as in Fig. 1.

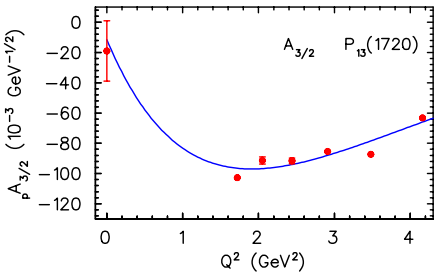

Fig. 7. Transverse form factor of the $P_{13}(1720)$ resonance. Notation as in Fig. 1.

4 Empirical transverse charge transition densities

In the following, we will consider the e.m. $\mathrm{N} \to \mathrm{N}^*$ transition when viewed from a light front moving towards the baryon. Equivalently, this corresponds with a frame where the baryons have a large momentum-component along the z-axis chosen along the direction of $P = (p + p')/2$, where p (p') are the initial (final) baryon four-momenta. We indicate the baryon light-front + component by P^+ (defining $a^\pm \equiv a^0 \pm a^3$). We can furthermore choose a symmetric frame where the virtual photon four-momentum q has $q^+ = 0$, and has a transverse component (lying in the xy-plane) indicated by the transverse vector $\vec{q}_\perp$, satisfying $q^2 = -\vec{q}_\perp^{\,2} \equiv -Q^2$. In such a symmetric frame, the virtual photon only couples to forward moving partons and the + component of the electromagnetic current J^+ has the interpretation of the quark charge density operator. It is given by $J^+(0) = +2/3\,\bar{u}(0)\gamma^+ u(0) - 1/3\,\bar{d}(0)\gamma^+ d(0)$, considering only u and d quarks. Each term in the expression is a positive operator since $\bar{q}\gamma^+ q \propto |\gamma^+ q|^2$.

We define a transition charge density for the unpolarized $\mathrm{N} \to \mathrm{N}^*$ transition by the Fourier transform

$$\rho_0^{\mathrm{NN}^*}(\vec{b}) \equiv \int \frac{\mathrm{d}^2\vec{q}_\perp}{(2\pi)^2}\, \mathrm{e}^{-\mathrm{i}\,\vec{q}_\perp\cdot\vec{b}}\, \frac{1}{2P^+} \times \left\langle P^+, \frac{\vec{q}_\perp}{2}, \lambda \,|\, J^+(0) \,|\, P^+, -\frac{\vec{q}_\perp}{2}, \lambda \right\rangle, \tag{7}$$

where λ denotes the nucleon and N* light-front helicities, $\vec{q}_\perp = Q(\cos\phi_q \hat{e}_x + \sin\phi_q \hat{e}_y)$, and where the 2-dimensional vector $\vec{b}$ denotes the position (in the xy-plane) from the transverse c.m. of the baryons.

First we will consider the case of $j = 1/2$ resonances, as P_{11} and S_{11}. These cases are very similar to the nucleon and can be worked out in an analogous way. The Fourier transform in Eq. (7) leads to

$$\rho_0^{NN^*}(\vec{b}) = \int_0^\infty \frac{dQ}{2\pi} Q\, J_0(bQ) F_1^{NN^*}(Q^2), \qquad (8)$$

where J_n denotes the cylindrical Bessel function of order n. Note that $\rho_0^{NN^*}$ only depends on $b = |\vec{b}|$. It has the interpretation of the quark (transition) charge density in the transverse plane which induces the N $\to$ N* excitation.

The above unpolarized transition charge density involves only one of the two independent N $\to$ N* e.m. form factors. To extract the information encoded in $F_2^{NN^*}$, we consider the transition charge densities for a transversely polarized N and N*. We denote this transverse polarization direction by $\vec{S}_\perp = \cos\phi_S \hat{e}_x + \sin\phi_S \hat{e}_y$. The transverse spin state can be expressed in terms of the light front helicity spinor states as $\left| s_\perp = +\frac{1}{2} \right\rangle = \left(\left| \lambda = +\frac{1}{2} \right\rangle + e^{i\phi_S} \left| \lambda = -\frac{1}{2} \right\rangle \right) / \sqrt{2}$, with $s_\perp$ the nucleon spin projection along the direction of $\vec{S}_\perp$.

We can then define a transition charge density for a transversely polarized N and N*, both along the direction of $\vec{S}_\perp$ as

$$\rho_T^{NN^*}(\vec{b}) \equiv \int \frac{d^2\vec{q}_\perp}{(2\pi)^2} e^{-i\vec{q}_\perp \cdot \vec{b}} \frac{1}{2P^+} \times \left\langle P^+, \frac{\vec{q}_\perp}{2}, s'_\perp \left| J^+(0) \right| P^+, -\frac{\vec{q}_\perp}{2}, s_\perp \right\rangle. \qquad (9)$$

Using Eq. (8), the Fourier transform of Eq. (9) can be worked out for the case $s'_\perp = s_\perp$ as

$$\rho_T^{NN^*}(\vec{b}) = \rho_0^{NN^*}(b) + \sin(\phi_b - \phi_S) \times \int_0^\infty \frac{dQ}{2\pi} \frac{Q^2}{(M^* + M_N)} J_1(bQ) F_2^{NN^*}(Q^2), \qquad (10)$$

where the second term, which describes the deviation from the circular symmetric unpolarized charge density, depends on the orientation of $\vec{b} = b(\cos\phi_b \hat{e}_x + \sin\phi_b \hat{e}_y)$. In the following we choose the transverse spin along the x-axis ($\phi_S = 0$).

In Fig. 8 we show the results for the N $\to P_{11}(1440)$ transition charge densities both for the unpolarized case and for the case of transverse polarization in for the proton and in Fig. 9 for the neutron. We use the empirical information on the N $\to$ N$^*(1440)$ transition FFs as given in our parametrization of this work.

It is seen that for the transition on a proton, which is well constrained by data, there is an inner region of positive quark charge concentrated within 0.5 fm, accompanied by a relatively broad band of negative charge extending out to about 1 fm.

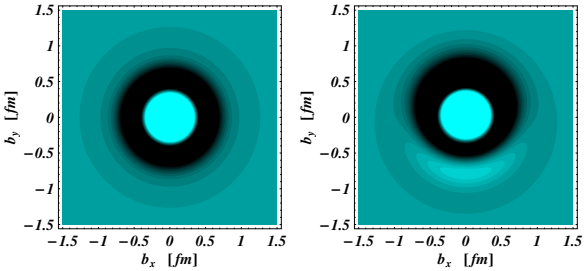

Fig. 8. Quark transverse charge density corresponding to the p $\to P_{11}(1440)$ e.m. transition. Left panel: When p and N* are unpolarized ($\rho_0^{pN^*}$). Right panel: When p and N* are polarized along the x-axis ($\rho_T^{pN^*}$). The light (dark) regions correspond with positive (negative) densities. For the p $\to P_{11}(1440)$ e.m. transition FFs, we use the improved MAID2008 fit of this work.

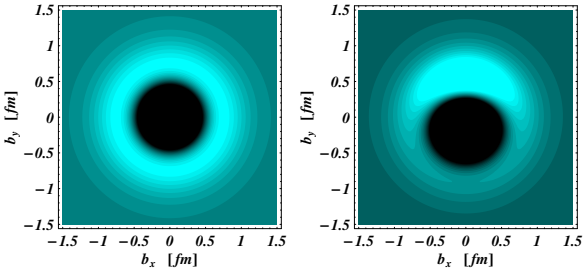

Fig. 9. Quark transverse charge density corresponding to the n $\to P_{11}(1440)$ e.m. transition. Left panel: When n and N* are unpolarized ($\rho_0^{nN^*}$). Right panel: When n and N* are polarized along the x-axis ($\rho_T^{nN^*}$). The light (dark) regions correspond with positive (negative) densities. For the n $\to P_{11}(1440)$ e.m. transition FFs, we use the MAID2007 fit.

When polarizing the baryon in the transverse plane, the large value of the magnetic transition strength at the real photon point, yields a sizeable shift of the charge distribution, inducing an electric dipole moment. For the neutron, which is not very well constrained by data, the MAID2007 analysis yields charge distributions of opposite sign compared to the proton, with active quarks spreading out over even larger spatial distances.

Figure 10 shows the unpolarized and polarized transition charge densities from the proton to the

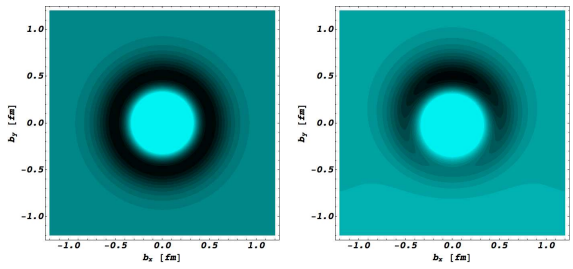

Fig. 10. Quark transverse charge density corresponding to the p $\to S_{11}(1535)$ e.m. transition. Left panel: When p and S_{11} are in a light-front helicity +1/2 state ($\rho_0^{pS_{11}}$). Right panel: When p and S_{11} are polarized along the x-axis with opposite spin projections ($\rho_T^{pS_{11}}$), i.e. $s_\perp = -s'_\perp = +1/2$. The light (dark) regions correspond with positive (negative) densities. For the p $\to S_{11}(1535)$ e.m. transition FFs, we use the MAID2007 fit.

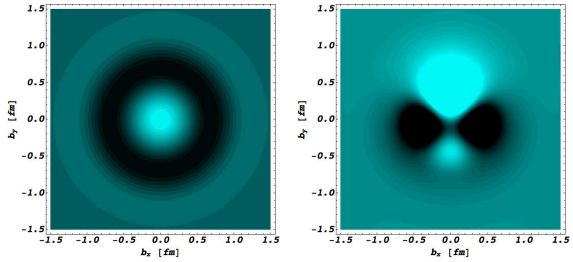

Fig. 11. Quark transverse charge density corresponding to the p $\to D_{13}(1520)$ e.m. transition. Left panel: When p and D_{13} are in a light-front helicity +1/2 state ($\rho_0^{pD_{13}}$). Right panel: When p and D_{13} are polarized along the x-axis with spin projections ($\rho_T^{pD_{13}}$) as in Fig. 10. The light (dark) regions correspond with positive (negative) densities. For the p $\to D_{13}(1520)$ e.m. transition FFs, we use the improved MAID2008 fit of this work.

$S_{11}(1535)$ resonance. It can be compared to the corresponding Fig. 8 for the Roper. The up quarks are not so strongly localized and also the ring of down quarks is less pronounced, in particular for the density corresponding to $F_2^{NN^*}$ in the second panel.

Finally, in Fig. 11 we show two transition densities from the proton to the $D_{13}(1520)$ resonance. Similar to the N$\Delta(1232)$ transition, also here we have 3 FFs leading to 3 densities.

The unpolarized density is similar to the Roper with, however, more diffuse boundaries between up and down quarks. In addition to the dipole transition density, in this case we also get a quadrupole density which is shown in the second panel.

5 Summary and conclusions

Using the world data base of pion photo- and electroproduction and recent data from Mainz, Bonn, Bates and JLab we have made a first attempt to extract all longitudinal and transverse helicity amplitudes of nucleon resonance excitation for four-star resonances below $W = 2$ GeV. For this purpose we have extended our unitary isobar model MAID and have parameterized the Q^2 dependence of the transition amplitudes. Comparisons between single-Q^2 fits and a Q^2 dependent superglobal fit give us confidence in the determination of the helicity couplings of the $P_{33}(1232)$, $P_{11}(1440)$, $S_{11}(1535)$, $D_{13}(1520)$ and the $F_{15}(1680)$ resonances, even though the model uncertainty of these amplitudes can be as large as 50% for the longitudinal amplitudes of the D_{13} and F_{15}.

These form factors were used to extract the quark transverse charge densities inducing these transitions. The rings of up and down quarks in these two-dimensional representations show very different structures for the Roper, the S_{11} and the D_{13} resonances.

References

1 Amsler C et al. Phys. Lett. B, 2008, **667**: 1; http://pdg.lbl.gov/
2 Miller G A. Phys. Rev. Lett., 2007, **99**: 112001
3 Carlson C E, Vanderhaeghen M. Phys. Rev. Lett., 2008, **100**: 032004
4 Carlson C E, Vanderhaeghen M. arXiv:0807.4537 [hep-ph]
5 Drechsel D, Kamalov S S, Tiator L. Eur. Phys. J. A, 2007, **34**: 69
6 Tiator L, Vanderhaeghen M. Phys. Lett. B, 2009, **672**: 344
7 Arndt R A, Strakovsky I I, Workman R L. Phys. Rev. C, 1996, **53**: 430; (SP99 solution of the GW/SAID analysis)
8 Drechsel D, Hanstein O, Kamalov S S, Tiator L. Nucl. Phys. A, 1999, **645**: 145; http://www.kph.uni-mainz.de/MAID/
9 Joo K et al. Phys. Rev. Lett., 2002, **88**: 122001-1
10 Joo K et al. Phys. Rev. C, 2004, **70**: 042201
11 Laveissiere G et al. Phys. Rev. C, 2004, **69**: 045202
12 Egiyan H et al. Phys. Rev. C, 2006, **73**: 025204
13 Ungaro M et al. Phys. Rev. Lett., 2006, **97**: 112003
14 Park K et al. Phys. Rev. C, 2008, **77**: 015208
15 Buchmann A J. Phys. Rev. Lett., 2004, **93**: 212301-1
16 JI X D, MA J P, YUAN F. Phys. Rev. Lett., 2003, **90**: 241601
17 LI Z P, Burkert V, LI Z J. Phys. Rev. D, 1992, **46**: 70
18 Aznauryan I G et al (CLAS Collaboration). Phys. Rev. C, 2008, **78**: 045209; and private communication